Eur. Phys. J. D **34**, 151–155 (2005)
DOI: 10.1140/epjd/e2005-00109-6

THE EUROPEAN PHYSICAL JOURNAL D

Time-dependent spectrum of thermionic emission from hot C_{60}

C. Bordas[a], B. Baguenard, B. Climen, M.A. Lebeault, F. Lépine, and F. Pagliarulo

Laboratoire de Spectrométrie Ionique et Moléculaire, CNRS UMR N° 5579 et Université Lyon I, Bât. Kastler 43, boulevard du 11 novembre 1918, 69622 Villeurbanne Cedex, France

Received 6 September 2004
Published online 13 July 2005 –

Abstract. Experimental measurements of time-dependent photoelectron spectra observed in thermionic emission of hot C_{60} excited by multiphoton absorption are presented. Time resolved velocity-map imaging is used to record photoelectron spectra and to disentangle direct and delayed processes. The evolution of the kinetic energy distribution of thermal electrons as a function of the delay after multiphoton excitation is described within the general formalism of the detailed balance theory. Experimental spectra obtained in the near-UV are in excellent agreement with the assumption of thermal equilibrium.

PACS. 36.40.-c Atomic and molecular clusters – 33.60.Cv Ultraviolet and vacuum ultraviolet photoelectron spectra

1 Introduction

Thermodynamics of finite-size systems is one of the many fields where the study of competing decay processes in excited clusters offers a renewed approach of the limit between bulk and diluted matter. Owing to various experimental factors, delayed electron emission [1] has focused a lot of interest. By analogy with bulk-matter, delayed electron emission from clusters [2–8] is described as thermionic emission when the excitation energy is equipartitioned between the electronic and nuclear degrees of freedom. Until recently, common photoelectron spectroscopy techniques provided only time-integrated photoelectron spectra [2–5] or measurements of the total photoelectron current as a function of time delay [6–8]. This appeared to be a serious limitation and only a complete approach, allowing the measurement of the kinetic energy distribution of the ejected electrons as a function of the delay after excitation, may provide a global understanding of thermionic emission. The widespread diffusion of charged particle imaging [9] and its intrinsic capability to combine energy and time resolution has allowed to circumvent this limitation. We have recently developed a spectrometer with time resolution based on velocity-map imaging [10]. This new spectrometer [11] has been applied to the study of thermionic emission, first reported in C_{60} [12].

Delayed ionization of C_{60} following excitation in the visible or near-UV has been a subject of increasing interest during the past decade [12–16]. In this spectral range, the multiphoton excitation process leads to a broad internal energy distribution of the excited sample. Owing to this broadband excitation, the emission current is described by a power law, as demonstrated by Hansen and Echt [17]. By contrast, experiments using the free-electron laser Felix [18,19] have shown that resonance enhanced multiphoton ionization (REMPI) in the infrared via a sequential vibrational excitation of C_{60} leads to a much narrower internal energy distribution owing to the very high-order of the process.

2 Outline of the detailed-balance theory

The decay mechanisms of excited clusters may be described in the framework of statistical mechanics using the detailed-balance theory introduced by Weisskopf [20]. A detailed description of this method is given in references [21–23]. Let us simply recall the main lines of the theoretical background. Based on the assumptions of statistical equilibrium and micro-reversibility of quantum processes, detailed-balance allows to express the differential thermionic emission rate of a system of internal energy E as follows:

$$k_{el}(E,\epsilon) = \frac{2m}{\pi^2\hbar^3}\sigma(\epsilon)\epsilon \exp\left(-\frac{\epsilon}{k_B T_d}\right)\exp\left(-\frac{\Phi}{k_B T_e}\right) \quad (1)$$

where ϵ is the electron kinetic energy, m and $\sigma(\epsilon)$ are respectively the electron mass, and the cross-section for electron capture, which depends explicitly on the nature of the interaction potential between the electron and the daughter fragment, Φ is the ionization potential. We have introduced the daughter temperature T_d, microcanonical temperature of the daughter system of internal energy $(E-\Phi)$. The differential rate depends explicitly on the capture cross-section and reflects the final temperature of

[a] e-mail: bordas@lasim.univ-lyon1.fr

the system. The emission temperature T_e has been introduced as the temperature of a system of internal energy $(E - \Phi/2)$. Integrating over ϵ, the microcanonical decay rate may be written in an Arrhenius form as follows:

$$K_{el}(E) = \omega(E) \exp\left(-\frac{\Phi}{k_B T_e}\right) \quad (2)$$

where the prefactor ω depends slowly on the energy E.

For a neutral system like C_{60}, the capture cross-section $\sigma(\epsilon)$ appearing in equation (1) may be evaluated according to standard approximations for Coulomb interaction [24] and the differential rate for thermionic emission may be expressed for a neutral system of radius R_0 as:

$$k_{el}(E,\epsilon) = \frac{2m}{\pi^2\hbar^3}\pi R_0^2(\epsilon + |V(R_0)|) \times \exp\left(-\frac{\epsilon}{k_B T_d}\right) \exp\left(-\frac{\Phi}{k_B T_e}\right) \quad (3)$$

where $V(R)$ is the Coulomb potential. In the low energy range of interest, and for a small particle radius equation (3) simplifies to:

$$k_{el}(E,\epsilon) \propto \exp\left(-\frac{\epsilon}{k_B T_d}\right). \quad (4)$$

Beside thermionic emission, the principal decay channel to be considered in the case of C_{60} is dissociation in $C_2 + C_{58}$. All other decay channels are neglected in the following. The total emission rate $K(E)$ is therefore the sum of the ionization rate $K_{el}(E)$ (Eq. (2)) and of the dissociation rate $K_{diss}(E)$. We express the dissociation rate as follows:

$$K_{diss}(E) = \omega_{diss}(E) \exp\left(-\frac{E_{diss}}{k_B T_e^{diss}}\right). \quad (5)$$

The prefactor $\omega_{diss}(E)$ is a slowly varying function, T_e^{diss} is the emission temperature relative to the dissociation energy E_{diss}. In the excitation energy range considered here, we estimate the dissociation rate based on the work of Lifshitz [25] using $\omega_{diss}(E) = 8 \times 10^{20}$ Hz and $E_{diss} = 10$ eV. The variation of the thermionic emission rate and of the dissociation rate as a function of the internal energy of C_{60} evaluated according to these procedures is plotted in Figure 1. Note that the combination of a large ionization potential with a large number of internal degrees of freedom implies that about 60 eV of internal energy are required in order to observe thermionic emission on the timescale of one microsecond. In this energy range, the decay of C_{60} occurs mainly by emission of C_2 fragments as it is clearly visible in Figure 1.

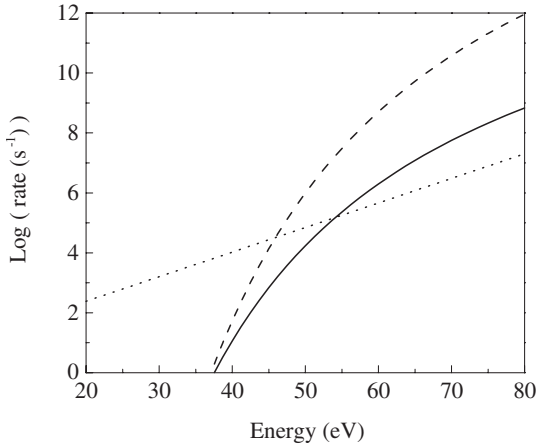

Fig. 1. Evolution of the decay rates as a function of the internal energy of C_{60}: thermionic emission rate calculated in the framework of the detailed-balance theory (solid-line); C_2 emission rate estimated according to reference [25] (dashed-line). For comparison, the blackbody radiation rate (dotted-line) [25] has been plotted; its contribution is negligible on the microsecond timescale.

3 Experimental set-up

A beam of cold C_{60} is produced by laser desorption of pure C_{60} embedded in a rod of organic material (matrix-assisted laser desorption). The optical excitation of the fullerenes is achieved in the interaction region of the velocity-map imaging spectrometer, which is also the extraction region of a time-of-flight ion mass spectrometer. Our experimental set-up allows the measurement of mass spectra (bearing the information relative to the decay rate) and of photoelectron spectra under strictly identical experimental conditions. Various experiments have been carried out in the range 220 to 400 nm, at laser fluences below 10^9 W/cm^2 (pulse duration 8 ns, 5 to 50 mJ per pulse). However, as mentioned above, owing to the large width of the internal energy distribution following multiphoton excitation in the visible or near-UV, these various experimental conditions do not lead to significant differences in the internal energy distribution of the molecules and the photoelectron spectra do not differ significantly as a function of the laser intensity or wavelength. While mass spectra are very sensitive to the excitation conditions (in particular the relative intensities of the various C_{60-2n}^+ fragment peaks) the photoelectron spectra are only slightly dependent on the excitation regime. At a given laser intensity, the energy distribution is well-described by a Poisson distribution. In the region of interest in the microsecond range i.e. around 60 eV, the width of the Poisson distribution is roughly $\langle E \rangle / \sqrt{N}$ i.e. about 15 eV. The emission is dominated by clusters having an internal energy such that the corresponding emission rate is the inverse of the observation window [23]. Provided the energy distribution is broad enough, the emission is consequently independent on the details of the distribution.

In order to measure photoelectron spectra as a function of the delay after excitation, we have developed a time-resolved velocity-map spectrometer [11] combining the position-sensitive-detection of the velocity-map imaging with electronic gating of the detector. The principle of photoelectron imaging spectroscopy is as follows. The optical excitation occurs in the center of the extraction region of the spectrometer. Photoelectrons ejected from

an atomic or molecular system are accelerated by an electric field onto a position-sensitive-detector (PSD). In our set-up, the PSD consists in a tandem microchannel-plates equipped with a phosphor screen for read-out. The amplified electron signal, converted to photons, is recorded via a digital CCD camera. The accumulation of electron impacts on the detector results in an image that contains the distribution of the projection of the initial velocity of the electrons onto the plane of detection. By choosing the laser polarization parallel to the detector plane, a simple inversion method [9,26] allows to extract the initial velocity distribution and therefore the energy spectrum. The electric field in the interaction region is tailored such that the electron impact position on the PSD depends only on its initial velocity irrespective of its initial position in the interaction region [10].

The time-of-flight of the electrons is essentially independent on the electron energy. As a consequence, the gating of the PSD allows the study of the evolution of the kinetic energy distribution of photoelectrons as a function of the time-delay after optical excitation. The time resolution of our spectrometer is limited to 50 ns, largely sufficient however for studying delayed ionization. This capability is a direct consequence of the purely geometrical measurement of the initial velocity, compatible with obtaining kinetic energy spectra for different time-windows after excitation. In addition, the detection efficiency of velocity-map imaging is constant at threshold, which is particularly useful for measuring the slow photoelectron energy distributions corresponding to thermal emission from hot clusters.

4 Experimental results

Figure 2 presents a typical time-of-flight mass spectrum obtained in multiphoton ionization of C_{60} at 330 nm. The broad peak of C_{60}^+ ions exhibits a long tail corresponding to delayed ionization extending beyond 10 μs. As stated above, owing to the broad internal energy distribution, the signal of delayed ionization is not exponential. Rather, it is a power law of time t^{-p}, with p being the ratio Φ/E_{diss}. The fragment peaks C_{58}^+, C_{56}^+, C_{54}^+, C_{52}^+, ... corresponding to successive loss of C_2 units are clearly visible. The signal of fragment ions does not exhibit a long tail. Therefore, electrons delayed by more than 200 ns arise entirely from C_{60} molecules, not from lighter fragments.

The experimental spectra presented in the following have all been obtained at a laser wavelength $\lambda = 330$ nm under moderate intensity. Notice that changing the wavelength in the range 220–400 nm does not change appreciably the experimental results, while changing the laser intensity strongly affect the time-of-flight spectrum (as the intensity increases, lighter fragments appear in the spectrum) without any significant change in the photoelectron kinetic energy distribution. Figure 3 presents a typical photoelectron spectrum resulting from the inversion of an electron image recorded without any gating on the detector. In addition to the integration of thermionic emission

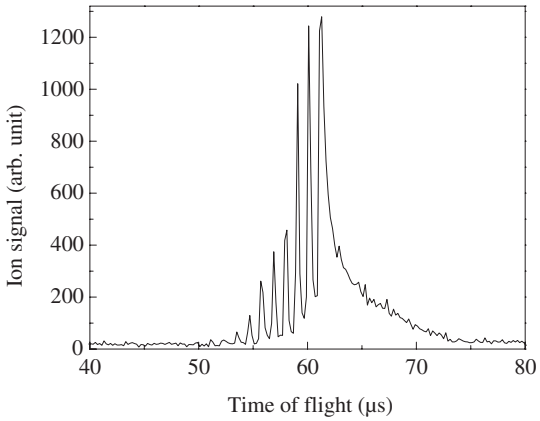

Fig. 2. Typical time-of-flight spectrum obtained by optical excitation of a beam of pure C_{60} at 330 nm at relatively low intensity. Fragments are ejected at short time-delays (narrow fragment peaks) while a long tail of thermionic emission of C_{60} is clearly visible on the most intense peak that extends beyond 10 μs after optical excitation.

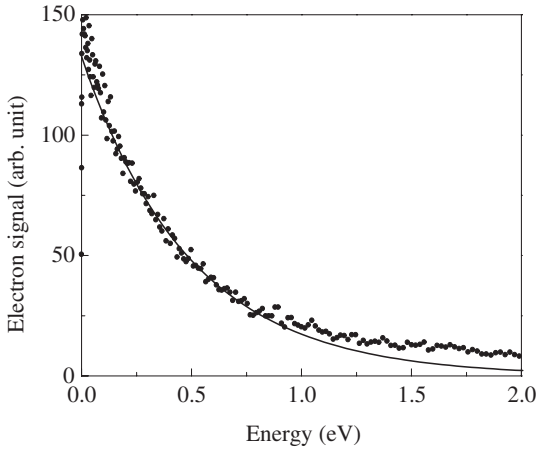

Fig. 3. Typical experimental spectrum (dots) obtained at a laser wavelength $\lambda = 330$ nm when integrating the photoelectron image over the whole decay process. Direct photoemission and thermionic emission from C_{60} are superimposed to other prompt electron emissions. No precise information may be drawn from such spectrum. The solid line is a fit to equation (4) that does not account for all contributions, especially above 1 eV.

over several μs, this spectrum also includes prompt electron emission processes occurring at short time-delay. The solid line represents a best-fit at low energy to the simple formula equation (4). There is obviously a stronger contribution at relatively high energy (above 1 eV) that cannot be attributed to thermionic emission. As a consequence, the effective temperature fitted on the experimental distribution of Figure 3 (almost 5000 K) is not relevant to a model including exclusively thermionic emission. Being the superimposition of different processes occurring on different timescales, this spectrum does not provide any conclusive information with regards to thermionic emission. Therefore, it is obvious that time-resolution is required in order to discriminate properly delayed electrons ejected

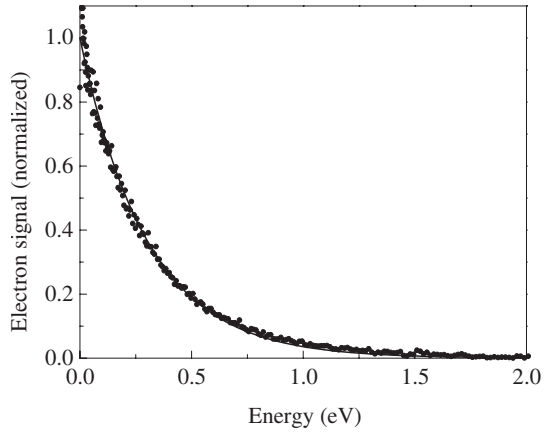

Fig. 4. Experimental spectrum recorded in the time range [200–300 ns] after excitation at $\lambda = 330$ nm (dots). An effective temperature of 3490±100 K is fitted (solid line) to the experimental distribution.

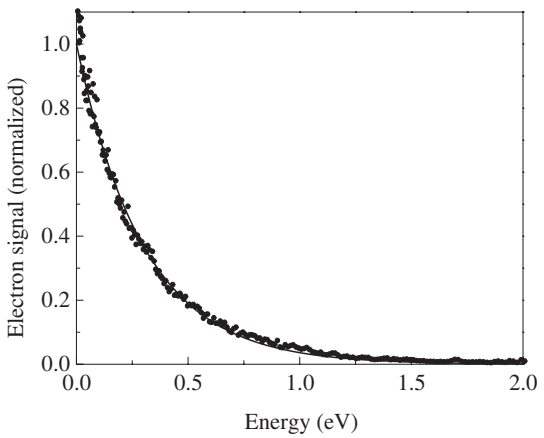

Fig. 5. Experimental spectrum recorded in the time range [1.0–1.1 μs] after excitation at $\lambda = 330$ nm (dots). An effective temperature of 3390±100 K is fitted (solid line) to the experimental distribution.

from C_{60} molecules from prompt electrons ejected from other species, in particular from super-excited fragments. As opposed to averaged spectra such as the one presented in Figure 3, time-resolved velocity-map-imaging allows to isolate properly photoelectrons emitted in a well defined delay window. Figure 4 presents such a spectrum recorded using a 100 ns-wide gate, at a time-delay of 200 ns after optical excitation. A least-square fitting of the spectrum with equation (4) (solid line) leads to an effective daughter temperature $T_d \approx 3490 \pm 100$ K. Notice the excellent agreement between experimental and calculated spectra. This excellent agreement confirms the validity of the detailed-balance model, and more importantly confirms that the assumption of thermal equilibrium is valid. Note also that the temperature fitted to our experimental data is in good agreement with other results obtained following a completely different experimental procedure by Tomita et al. [27]. As predicted by the model [23] and owing to the fast variation of the emission rate as a function of the internal energy, the evolution of the photoelectron spectrum with time delay is found to be rather slow. Indeed, the observation time-window is roughly the inverse of the emission rate of systems that contribute mainly to the electron emission in this given time-window. Therefore a significant variation in rate (i.e. in time-delay) corresponds only to a slight variation in temperature (i.e. in internal energy). This is clearly visible in Figure 5 where we have plotted a spectrum in the delay range [1.0–1.1 μs] under similar experimental conditions as in Figure 4. In that case, the effective temperature is slightly lower ($T_d \approx 3390 \pm 100$ K), however not sufficiently to draw any indication on the variation of the daughter temperature as a function of time-delay.

The present experimental results illustrate the validity of our approach. As opposed to experiments limited to total photoelectron current vs. time, these results allow to identify precisely thermionic emission and show that supplementary information may be extracted from the evolution of the photoelectron spectrum as a function of the delay after excitation. However, owing to the broad internal energy distribution inherent to the multiphoton excitation process in the near-UV range, initial experimental conditions cannot be significantly qualitatively varied. This is of course a strong limitation in these experiments: no matter the excitation scheme in the visible or near-UV the internal energy distribution is so broad that we have almost no experimental control on the degree of excitation of the fullerenes. There is however an alternative to this limitation if the excitation is performed in the infrared [18,19]. Experiments combining the free-electron laser Felix, with time-resolved velocity-map imaging are presently under way. Preliminary results in the mid-infrared exhibit a strong deviation from the simple formula equation (4) and tend to show that the assumption of thermal equilibrium may depend strongly on the nature of the excitation process.

5 Conclusion

Time-dependent photoelectron imaging has allowed us to discriminate without ambiguity between fast and delayed processes. Combined with the description of thermionic emission in the framework of the detailed-balance theory, a detailed understanding of the decay processes as well as a confirmation of simple law for photoelectron kinetic energy distribution in case of thermal equilibrium have been obtained. However, a number of points remain to be elucidated among which one may cite the understanding of the detailed mechanisms of thermalization under various excitation conditions and the behavior at large delays where blackbody radiation becomes the dominant decay process.

We acknowledge the support of the European Commission in the framework of the European Cluster Cooling Network (Contract No: HPRN-CT-2000-00026).

References

1. E.E.B. Campbell, R.D. Levine, Annu. Rev. Phys. Chem. **51**, 65 (2000)
2. G. Gantefor, W. Eberhardt, H. Weidele, D. Kreisle, E. Recknagel, Phys. Rev. Lett. **77**, 4524 (1996)
3. J.C. Pinaré, B. Baguenard, C. Bordas, M. Broyer, Phys. Rev. Lett. **81**, 2225 (1998)
4. B. Baguenard, J.C. Pinaré, F. Lépine, C. Bordas, M. Broyer, Chem. Phys. Lett. **352**, 14 (2002)
5. D. Ding, R.N. Compton, R.E. Haufler, C.E. Klots, J. Phys. Chem. **97**, 2500 (1993)
6. T. Leisner, K. Athanassenas, D. Kreisle, E. Recknagel, O. Echt, J. Chem. Phys. **99**, 9670 (1993)
7. S.E. Kooi, A.W. Castleman Jr., J. Chem. Phys. **108**, 8864 (1998)
8. B.A. Collings, A.H. Amrein, D.M. Rayner, P.A. Hackett, J. Chem. Phys. **99**, 4174 (1993)
9. *Imaging in Molecular Dynamics*, edited by B.J. Whitaker (Cambridge University Press, 2003)
10. A.T.J.B. Eppink, D.H. Parker, Rev. Sci. Instrum. **68**, 3477 (1997)
11. B. Baguenard, J.B. Wills, F. Pagliarulo, F. Lépine, B. Climen, M. Barbaire, C. Clavier, M.A. Lebeault, C. Bordas, Rev. Sci. Instrum. **75**, 324 (2004)
12. F. Lépine, B. Climen, F. Pagliarulo, B. Baguenard, M.-A. Lebeault, C. Bordas, M. Hedén, Eur. Phys. J. D **24**, 393 (2003)
13. E.E.B. Campbell, G. Ulmer, I.V. Hertel, Phys. Rev. Lett. **67**, 1986 (1991)
14. P. Sandler, C. Lifshitz, C.E. Klots, Chem. Phys. Lett. **200**, 445 (1992)
15. Y. Zhang, M. Stuke, Phys. Rev. Lett. **70**, 323 (1993)
16. D. Ding, J. Huang, R.N. Compton, C.E. Klots, R.E. Haufler, Phys. Rev. Lett. **73**, 1084 (1994)
17. K. Hansen, O. Echt, Phys. Rev. Lett. **78**, 2337 (1997)
18. G. von Helden, I. Holleman, G.M.H. Knippels, A.F.G. van der Meer, G. Meijer, Phys. Rev. Lett. **79**, 5234 (1997)
19. G. von Helden, I. Holleman, A.J.A. van Roij, G.M.H. Knippels, A.F.G. van der Meer, G. Meijer, Phys. Rev. Lett. **81**, 1825 (1998)
20. V. Weisskopf, Phys. Rev. **52**, 295 (1937)
21. J.U. Andersen, C. Gottrup, K. Hansen, P. Hvelplund, M.O. Larsson, Eur. Phys. J. D **17**, 189 (2001)
22. J.U. Andersen, E. Bonderup, K. Hansen, J. Phys. B **35**, R1 (2002)
23. F. Lépine, C. Bordas, Phys. Rev. A **69**, 053201 (2004)
24. C.E. Klots, J. Chem. Phys. **100**, 1035 (1994)
25. C. Lifshitz, Int. J. Mass. Spec. **198**, 1 (2000)
26. C. Bordas, F. Paulig, H. Helm, D.L. Huestis, Rev. Sci. Instrum. **67**, 2257 (1996)
27. S. Tomita, J.U. Andersen, K. Hansen, P. Hvelplund, Chem. Phys. Lett. **382**, 120 (2003)